MRI-Based Radiomics Signature: A Potential Biomarker for Identifying Glypican 3-Positive Hepatocellular Carcinoma

Dongsheng Gu, PhD,[1] Yongsheng Xie, MD,[3†] Jingwei Wei, PhD,[1] Wencui Li, MD,[3†]

Zhaoxiang Ye, PhD,[3] Zhongyuan Zhu, MD,[3] Jie Tian, PhD,[1,2,4,5*] ⃝ and Xubin Li, PhD[3*]

Background: Glypican 3 (GPC3) expression has proved to be a critical risk factor related to prognosis in hepatocellular carcinoma (HCC) patients.
Purpose: To investigate the performance of MRI-based radiomics signature in identifying GPC3-positive HCC.
Study Type: Retrospective.
Population: An initial cohort of 293 patients with pathologically confirmed HCC was involved in this study, and patients were randomly divided into training (195) and validation (98) cohorts.
Field Strength/Sequences: Contrast-enhanced T_1-weight MRI was performed with a 1.5T scanner.
Assessment: A total of 853 radiomic features were extracted from the volume imaging. Univariate analysis and Fisher scoring were utilized for feature reduction. Subsequently, forward stepwise feature selection and radiomics signature building were performed based on a support vector machine (SVM). Incorporating independent risk factors, a combined nomogram was developed by multivariable logistic regression modeling.
Statistical Tests: The predictive performance of the nomogram was calculated using the area under the receive operating characteristic curve (AUC). Decision curve analysis (DCA) was applied to estimate the clinical usefulness.
Results: The radiomics signature consisting of 10 selected features achieved good prediction efficacy (training cohort: AUC = 0.879, validation cohort: AUC = 0.871). Additionally, the combined nomogram integrating independent clinical risk factor α-fetoprotein (AFP) and radiomics signature showed improved calibration and prominent predictive performance with AUCs of 0.926 and 0.914 in the training and validation cohorts, respectively.
Data Conclusion: The proposed MR-based radiomics signature is strongly related to GPC3-positive. The combined nomogram incorporating AFP and radiomics signature may provide an effective tool for noninvasive and individualized prediction of GPC3-positive in patients with HCC.

*Address reprint requests to: X.L., Department of Radiology, Tianjin Medical University Cancer Institute and Hospital, National Clinical Research center for Cancer, Tianjin's Clinical Research Center for Cancer, Key Laboratory of Cancer Prevention and Therapy, Tianjin, China E-mail: lixb@bjmu.edu.cn or J.T., Key Laboratory of Molecular Imaging, Institute of Automation, Chinese Academy of Sciences, Beijing,China E-mail: tian@ieee.org
†Dongsheng Gu, Yongsheng Xie, Jingwei Wei and Wencui Li contributed equally to this work.

From the [1]Key Laboratory of Molecular Imaging, Institute of Automation, Chinese Academy of Sciences, Beijing, China; [2]University of Chinese Academy of Sciences, Beijing, China; [3]Department of Radiology, Tianjin Medical University Cancer Institute and Hospital, National Clinical Research center for Cancer, Tianjin's Clinical Research Center for Cancer, Key Laboratory of Cancer Prevention and Therapy, Tianjin, China; [4]Beijing Advanced Innovation Center for Big Data-Based Precision Medicine, School of Medicine, Beihang University, Beijing, China; and [5]Engineering Research Center of Molecular and Neuro Imaging of Ministry of Education, School of Life Science and Technology, Xidian University, Xi'an, China

Additional supporting information may be found in the online version of this article

HEPATOCELLULAR CARCINOMA (HCC) is the most common primary hepatic malignancy and the second cause of cancer mortality worldwide.[1] The prognosis of HCC has improved with advances in surgical resection and imaging technology; however, there still remains a high intrahepatic recurrence after hepatic resection.[2] Glypican 3 (GPC3) is a 70 kDa cell-surface protein that belongs to heparan sulfate proteoglycans and takes part in cellular growth, migration, and differentiation.[3,4] GPC3 is highly expressed in HCC tissues but is negative in benign hepatic diseases and adjacent normal liver tissue.[5]

Among the prognosis factors of HCC, GPC3 has been shown to be closely related to metastasis/recurrence in patients with HCC after operation.[6] Indeed, GPC3 expression in HCC is a significant independent factor predicting the poor prognosis for patients. GPC3 is involved in cellular growth, migration, and differentiation. It may contribute to angiogenesis, invasion, and apoptosis, possibly through its interactions with the Wnt and Hedgehog pathways.[7,8] Moreover, GPC3 has great promise to be an immunotherapeutic target in monoclonal antibody-based HCC therapy, especially for patients with advanced unresectable HCC and portal vein tumor thrombus.[9] Thus, in order to choose an optimal treatment strategy, it is key to identify GPC3-positive HCCs as early as possible.

One of the procedures for preoperative evaluation of CPC3 is fine-needle biopsy. But as an invasive method and has occasional complications, such as hemorrhage, local pain, and pneumothorax.[10] Additionally, the relationship between tumor and peritumoral hepatic tissues cannot be adequately assessed with a biopsy specimen due to unavoidable sampling error.[11] Fine-needle biopsy does not reflect the heterogeneity of the entire tumor, and thus could lead to a false-negative result of GPC3 expression. GPC3 can also be detected in the serum of HCC patients, but the detection rate is limited.[8] In addition, the reported serum GPC3 levels in HCC and normal subjects were variable among previous studies.[12–14] This may suggest that an accurate result cannot be achieved when detecting GPC3 in serum. For the abovementioned reasons, we proposed to identify GPC3-positive HCC patients through the use of noninvasive medical imaging.

Radiomics analysis with medical images has attracted attention as an emerging technique in medical imaging analysis in recent years.[15,16] Radiomics can obtain a variety of high-dimensional minable features that cannot be found with human vision via a high-throughput extraction algorithm.[17,18] These features may have the potential to capture intratumor heterogeneity, which can reflect the tumor tissue microenvironment and the cancer phenotype.[15] Recently, magnetic resonance imaging (MRI) has been successfully applied in predicting the pathological grading of tumor, assessing the malignancy and treatment response due to its advantages of multiparametric, multiorientation imaging and the high contrast of soft tissues.[19–22] It was reported that the radiomics signature based on contrast-enhanced MRI could act as an imaging biomarker to predict the microvascular invasion of HCC.[23] However, to our best knowledge, few studies have attempted to identify GPC3-positive HCC with a radiomics signature.

Therefore, we aimed to investigate the performance of a radiomics signature in identifying GPC3-positive HCC based on contrast-enhanced MR images in this study.

Materials and Methods

Study Population and MRI Protocol

This study was approved by our Institutional Review Board and written informed consent was waived for all participants. Patient medical records were reviewed to identify the patients who underwent liver dynamic MRI and subsequently underwent liver resection for HCC at our institution between April 2014 and December 2017. The subject inclusion criteria were as follows: 1) patients had single HCC at preoperative MRI; 2) patients had liver MRI with optimal image quality; 3) an interval of less than 1 month between MR examination and surgery; and 4) a pathologic report of HCC and underwent routine immunochemical staining for GPC3. The exclusion criteria for patients included: i) HCC lesion determined by three experienced radiologists was too small to displayed clearly on MRI; or ii) patients received treatment previously, such as transcatheter arterial chemoembolization, partial hepatectomy, chemotherapy, radiation therapy, or needle biopsy. According to pathologic reports, all participants with a single HCC were categorized by the presence or absence of GPC3 expression on immunochemical staining. Finally, a total of 293 HCC lesions in 293 patients (241 males and 52 females; mean age, 56.4± 10.0 years; range, 23–86 years) were identified in this study, consisting of 203 patients with HCCs positive for GPC3 and 90 patients with HCCs negative for GPC3. All 293 patients were divided randomly into two groups at a ratio 2:1, including a training cohort with 195 patients (160 males and 35 females; mean age, 56.2± 10.3 years; range, 23–86 years) and a validation cohort with 98 patients (81 males and 17 females; mean age, 57.0± 9.3 years; range, 29–76 years). We used all the MR images that had been archived in the hospital's picture archiving and communication system (PACS). The detailed MRI protocol is explained in Supplementary Method 1.

Workflow

The radiomics workflow is summarized in Fig. 1, including tumor segmentation, feature extraction, radiomics signature modeling, and model analysis. First, a region of interest (ROI) was delineated manually along the contours of the HCC lesions on each axial slice. Then high-dimensional shape, intensity, and textural and wavelet features were extracted. Next, feature selection and modeling were performed for the development of the radiomics signature. Finally, model analysis with different metrics evaluated the performance of the developed models.

ROI Placement and Feature Extraction

Detailed descriptions of ROI placement and feature extraction are presented in Supplementary Method 2. All the feature definition
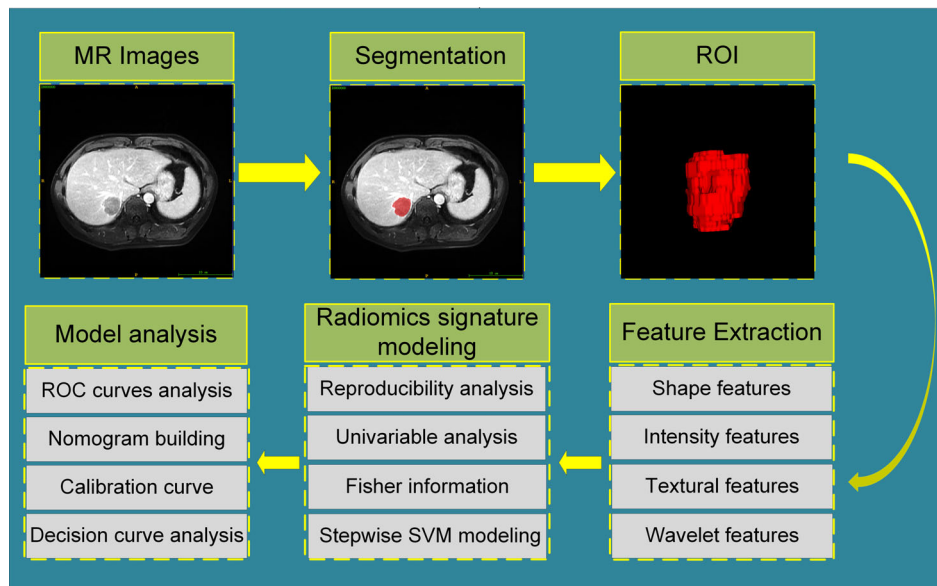
FIGURE 1: Workflow for the radiomics analysis

and extractions were performed by the guidelines of the Image Bio-marker Standardisation Initiative.[24] The processes of ROI placement and feature extraction were performed on the whole cohort.

Radiomics Feature Selection and Signature Modeling

In order to eliminate the effect of dimension differences of data, all radiomic features were normalized to zero-mean and unit-variance, with further analysis performed on these transformed variables. First, a reproducibility analysis with 20 repeated segmented lesions was performed to remove unstable features; the common features that have reproducibility in both intra- and interobserver were adopted. Second, univariable analysis with the Mann–Whitney U-test was performed for each radiomic feature. Next, Fisher information was conducted to determine the score of each feature. Finally, a support vector machine (SVM) classifier was utilized for radiomics modeling. The detailed processes including radiomics feature selection and sig-nature modeling are described in Supplementary Method 3. All the processes were implemented in the training cohort.

Nomogram Development and Validation

A combined model integrating clinical risk factors and radiomics sig-nature with backward stepwise multivariable logistic regression analy-sis was constructed using the training cohort data. In addition, to provide an individual predictive graphical presentation, a nomogram for the combined multivariable model was developed. The nomo-gram could help calculate the predicted probability of GPC3-positive for each individual patient. Furthermore, the calibra-tion performance was assessed with the Hosmer–Lemeshow test.[25] Decision curve analysis was performed to validate the clinical utility of the nomogram.[26] Net benefits at different thresholds were derived by calculating the difference between the true-positive rate and false-positive rate.

Model Evaluation and Comparison

The performance of the clinical model, radiomics signature, and combined model were evaluated by receiver operating characteristics curve (ROC) analysis in both the training and validation cohorts. The predictive accuracy of each model was quantified with the area under the curve (AUC). We compared different predictive perfor-mance using the Delong test. The best cutoff value calculated with Youden's index of the predictive probability for each model in the training cohort was given for classification of GPC3-positive and -negative.[27] Then, compared with the true GPC3 results, we calcu-lated the evaluation indices of accuracy, sensitivity, and specificity. A stratification analysis of the predictive nomogram in patients grouped by age and sex was validated.

Model Robustness Test

To validate the robustness and reliability of the developed models and results, we performed additional 10-fold cross-validation using the whole cohort. The whole cohort was randomly partitioned into 10 equal-size subsamples. The same processes of feature analysis and model building were executed on nine subsamples (training data) and validated on the remaining one subsample (validation data). We repeated this procedure 10 times and ensured that each of the 10 subsamples was used exactly once as the validation data.

Statistical Analysis

Univariable statistics analysis was performed for the clinicopathologic risk factor selection. First, the normality assumption was tested for each quantitative variable. Then, association between the quantita-tive clinicopathologic factor and GPC3 was evaluated with a t-test for variables in normal distribution or Mann–Whitney U-test for variables in nonnormal distribution. Moreover, a qualitative clinico-pathologic factor was evaluated using the chi-square test. Variables with $P < 0.05$ in a statistics test in the training cohort was consid-ered significantly related to GPC3, and subsequently entered into a backward stepwise multivariable logistic regression analysis with the

likelihood ratio test. Finally, the remaining variables after the multi-variable analysis were regarded as potential risk factors and included for clinical modeling in the training cohort.

Statistical analyses in this study were conducted with the software IBM SPSS Statistics v. 20.0 (Armonk, NY) and R software (v. 3.5.0, Vienna, Austria). A detailed description for R packages used in statistics analysis are listed in Supplementary Method 4.

Results

Clinicopathologic Characteristics and Clinical Modeling

The preoperative clinicopathologic information between GPC3-positive and GPC3-negative patients in both training and validation dataset are shown in Table 1. No significant differences were observed between the training and validation cohorts through all the clinical factors with P-values ranging from 0.102 to 0.978.

Univariate analysis in the training cohort showed that age, diameter, α-fetoprotein (AFP), total bilirubin (TBIL), and hepatitis were significantly association with GPC3 ($P < 0.05$ in all cases). All the significant factors were entered into the backward stepwise multivariable logistic regression analysis. Finally, the diameter (odds ratio [OR] = 0.978; 95% concordance index [CI]: 0.967–0.989, $P < 0.05$) and AFP (OR = 4.311; 95% CI: 2.540–7.319; $P < 0.05$) were considered the independent risk factors for clinical model building with logistic regression, while the age, TBIL, and hepatitis were filtered out in the analysis. The clinical model yielded an AUC of 0.815 (95% CI: 0.752–0.878) in the training cohort and 0.758 (95% CI: 0.661–0.855) in the validation cohort (Fig. 2).

Feature Selection and Radiomics Signature Development

After the feature robustness analysis (Figure S1), we derived 215 and 224 radiomic features with intra- and inter-correlation coefficients greater than 0.75 separately. Then the 180 robust features were adopted. Univariate analysis showed that 168 features were significantly different between GPC3-positive and GPC3-negative groups. Fisher scores of the top-ranked 20 features are presented in Figure S2, and the results of mean cross-validation AUCs with different feature numbers are plotted in Figure S3. It can be concluded from the curve that the SVM classifier obtained the best discrimination performance, with 10 features. The visualization of the first-order statistical radiomics feature is shown in Figure S4.

Diagnosis of Radiomics Signature

The radiomics signature showed a good discrimination ability for GPC3 with an AUC of 0.879 (95% CI, 0.822–0.936) in the training cohort and 0.871 (95% CI, 0.783–0.960) in the validation cohort (Fig 2a,b). Meanwhile, the radiomics signature for individual patients in both the GPC3-positive and GPC3-negative groups are shown in Fig. 3a,b, indicating a significant distribution difference ($P < 0.05$). Calculated with the Youden Index, the best cutoff value of the radiomics signature was 0.539. Classified by the cutoff value, an accuracy of 83.1% and 75.5% were obtained in the training and validation cohorts, respectively. Detailed predictive performance of the radiomics signature is shown in Table 2.

Performance of the Combined Model

After the backward stepwise selection, the AFP and radiomics signature were selected as significant predictors for GPC3 and remained in the combined model. The combined model yielded an AUC of 0.926 (95% CI, 0.884–0.969) in the training cohort, and an AUC of 0.914 (95% CI, 0.848–0.980) in the validation cohort, which were significantly better than the clinical results ($P < 0.05$). Moreover, the model had good accuracies for predicting the GPC3 in the training (accuracy: 86.7%; sensitivity: 86.7%, specificity: 86.7%) and the validation (accuracy: 79.6%; sensitivity: 73.5%, specificity: 93.3%) cohorts (Table 2). Stratification analysis also showed good performance in both subgroups of age and sex (Table S1). ROC curves of the clinical model, radiomics signature, and combined models are shown in Fig. 2. The classification results for all the patients of each model are presented in Table S2. The results of robustness and the reliability test of the developed models with 10-fold cross-validation are shown in Tables S3 and S4. Stable and powerful prediction performance of the combined model in training cohort (mean AUC± standard deviation [SD], 0.939 ± 0.011) and validation cohort (mean AUC±SD, 0.921 ± 0.027) were obtained.

Development and Validation of the Nomogram

The developed nomogram is shown in Fig. 4a. The distribution of our nomogram predicted probabilities for each patient with the recommend threshold in GPC3-positive and GPC3-negative groups is presented in Fig. 3c,d. The threshold to differentiate GPC3 was 0.703 as calculated by the Youden Index. Calibration curves are shown in Fig. 4b,c, with good agreement in both the training ($P > 0.221$) and the validation ($P > 0.394$) cohorts. The results of the decision curve analysis for clinical and combined models are shown in Fig. 5. The predictive nomogram obtained more net benefits than the clinical model and "treat-all" or "treat-none" strategies for most of the threshold probabilities ($P > 1\%$).

Discussion

In this retrospective study we proposed and validated a combined nomogram that could preoperatively diagnose GPC3-positive HCC patients with MR images. The combined nomogram, integrating the radiomics signature and clinical risk factor AFP, showed more competitive

TABLE 1. Patient Characteristics in the Training and Validation Cohorts

Characteristics	Training dataset (N = 195)			Validation dataset (N = 98)			P
	GPC3 (+)	GPC3 (−)	P	GPC3 (+)	GPC3 (−)	P	
Age (years)	55±10	60±9	<0.05	55±9	60±9	0.061	0.526
Diameter (mm)	50±31	66±33	<0.05	55±34	56±30	0.989	0.922
ALT (U/L)	44±64	45±36	0.883	42±33	39±30	0.606	0.628
Sex			0.926			0.645	0.899
Male	111 (82.2)	49 (81.7)		57 (83.8)	24 (80.0)		
Female	24 (17.8)	11 (18.3)		11 (16.2)	6 (20.0)		
AFP (ng/ml)			<0.05			<0.05	0.730
<20	42 (31.1)	43 (71.7)		22 (32.4)	22 (73.3)		
20–400	34 (25.2)	12 (20.0)		20 (29.4)	6 (20.0)		
>400	59 (43.7)	5 (8.3)		26 (38.2)	2 (6.7)		
ALB (g/L)			0.128			0.773	0.227
<40	29 (21.5)	19 (31.7)		13 (19.1)	5 (16.7)		
>40	106 (78.5)	41 (68.3)		55 (80.9)	25 (83.3)		
TBIL (µmol/L)			<0.05			0.050	0.827
<21	97 (71.9)	52 (86.7)		49 (72.1)	27 (90.0)		
>21	38 (28.1)	8 (13.3)		19 (27.9)	3 (10.0)		
Hepatitis			<0.05			0.367	0.517
Absent	37 (27.4)	28 (46.7)		22 (32.4)	7 (23.3)		
Present	98 (72.6)	32 (53.3)		46 (67.6)	23 (76.7)		
Cirrhosis			0.060			0.609	0.102
Absent	28 (20.7)	20 (33.3)		24 (35.3)	9 (30.0)		
Present	107 (79.3)	40 (66.7)		44 (64.7)	21 (70.0)		
Ascites			0.672			0.381	0.896
Absent	112 (83.0)	52 (86.7)		59 (86.8)	24 (80.0)		
Present	23 (17.0)	8 (13.3)		9 (13.2)	6 (20.0)		
Total	135 (69.2)	60 (30.8)	—	68 (69.4)	30 (30.6)	—	0.978

GPC3 (+), GPC3-positive; GPC3 (−), GPC3-negative; ALT, alanine aminotransferase; AFP, α-fetoprotein; albumin, ALB; TBIL, total bilirubin. Qualitative variables are in n (%) and analyzed using the chi-square or Fisher's exact tests, while quantitative variables are in mean±SD and analyzed using t-test or Mann–Whitney U-test, as appropriate. P represents the result of statistics test between GPC3 (+) and GPC3 (−). P represents the results of statistics test between the training and validation cohorts.

performance in the training and validation cohorts compared with the clinical and radiomic predictive models alone. Moreover, nomograms displayed high sensitivity in both patient cohorts, which suggested a higher detected rate of GPC3-postive, especially compared with the serum screening for GPC3.[5] Thus, we consider the nomogram as an effective tool for preoperative noninvasive and individualized prediction of GPC3-positive in HCC patients.

GPC3 has become a novel tumor biomarker for HCC since first identified in 1988 by Filmus et al.[28] Although GPC3 has been explored as a clinical diagnostic factor for HCC in many previous studies, few studies proposed effective
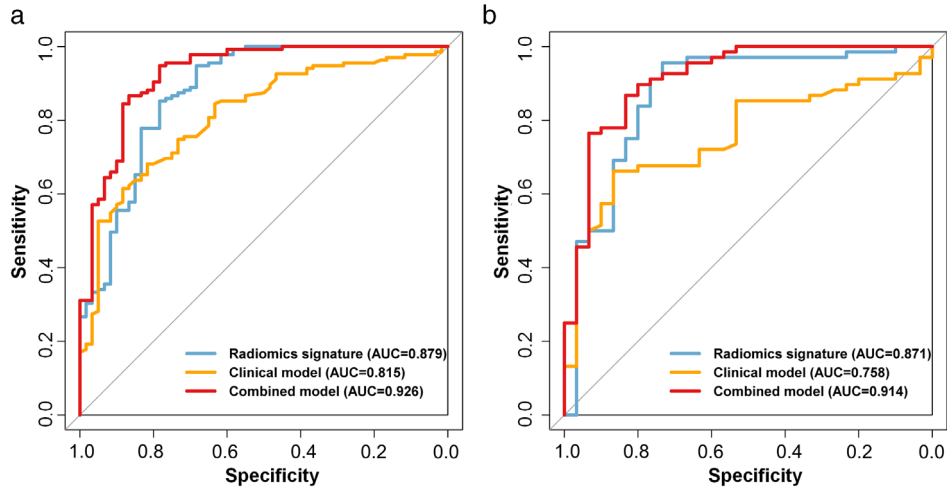
FIGURE 2: Comparison of receiver operating characteristics (ROC) curves for prediction of GPC-3 expression. ROC curves of the radiomics signature, clinical model, and combined model in training (a) and validation (b) cohorts
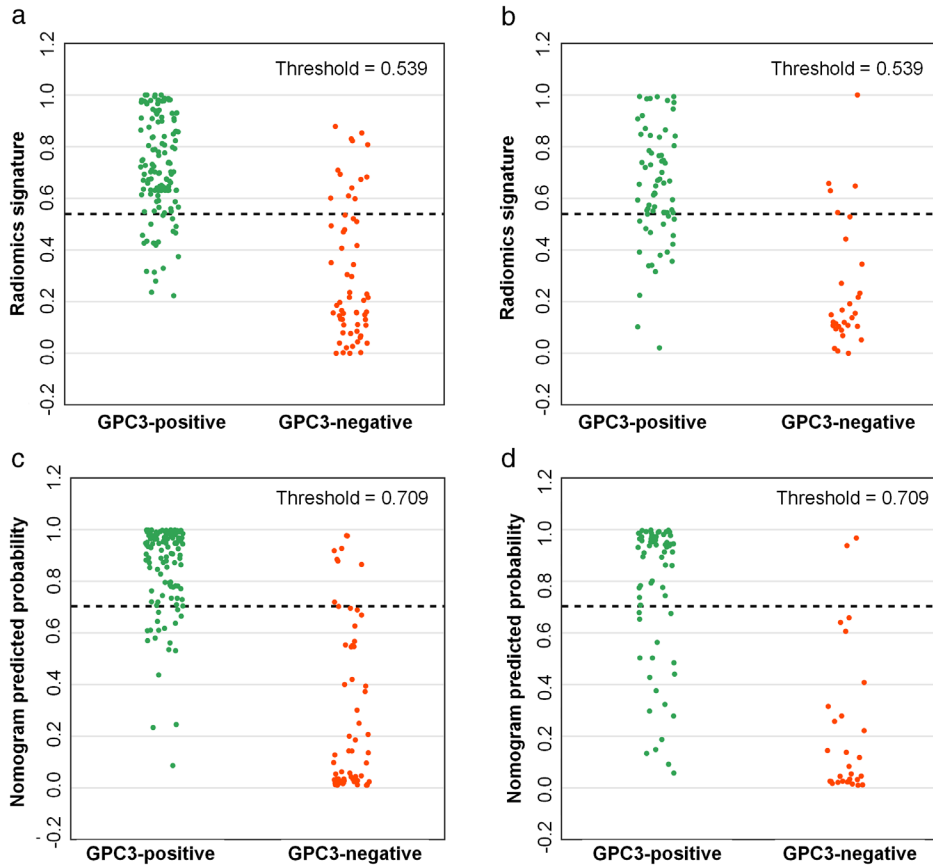

FIGURE 3: The predicted distribution of patients in GPC3-positive and GPC3-negative groups. The radiomics signature for individual patients in GPC3-positive and GPC3-negative groups in the training (a) and validation (b) cohorts. The predicted probabilities of nomogram for individual patients in GPC3-positive and GPC3-negative groups in the training (c) and validation (d) cohorts. The dashed lines represent the thresholds used for the classification of GPC3 expression for each patient

quantitative predictors to identify GPC3 expression. Fu et al explored the relationship between 15 clinicopathologic characteristics and GPC3 expression, finding that tumor number, AFP level, and TNM stage were significantly associated with GPC3.[29] Yasuda et al found that GPC3 expression tended to

increase with decreasing differentiation of HCC.[30] However, these studies did only a statistical correlation analysis without developing a model and assessing the predicted performance.

In this work we utilized radiomic features of the 3D primary tumor to predict GPC3-positive in HCC. Compared

TABLE 2. Predictive Performance for the Proposed Models

Different models	Training dataset N = 195				Validation dataset N = 98				
	AUC (95% CI)	ACC	SENS	SPEC	AUC (95% CI)	ACC	SENS	SPEC	Cutoff
Clinical model	0.815 (0.752–0.878)	72.3%	68.2%	81.7%	0.758 (0.661–0.855)	71.4%	67.7%	80.0%	0.648
Radiomics signature	0.879 (0.822–0.936)	83.1%	85.2%	78.3%	0.871 (0.783–0.960)	75.5%	72.1%	83.3%	0.539
Combined model	0.926 (0.884–0.969)	86.7%	86.7%	86.7%	0.914 (0.848–0.980)	79.6%	73.5%	93.3%	0.703

AUC: area under the curve; CI: confidence interval; ACC: accuracy; SENS: sensitivity; SPEC: specificity.

with 2D tumor slice, the 3D tumor volume might provide more complete shape information and contain more representative information of tumor heterogeneity.[31,32]

In the analysis presented here, all of the selected features were wavelet features derived from imaging after wavelet filtering; this indicated the effectiveness of wavelet decompositions from the original image. The features in the wavelet domain focused on different frequency ranges, which can distinguish the difference of the tumor microenvironment.[15] Specifically, tumor features with high frequency reflected the tumor edge and detailed information, while features with low frequency obtained the tumor outline information and filtered the noise at the same time. Furthermore, we discovered one feature, "wavelet-HLH_firstorder_Range," that corresponded to the biological characteristics. The range of the intensity histogram represents the discrete degree of gray level in different tumor areas on the image, and the variance between the GPC3-positive and GPC3-negative HCC could be attributed to intratumoral heterogeneity (eg, angiogenesis, invasion, and apoptosis) involved with GPC3 expression.[7,8]

During the construction of the clinical model, the potential clinical risk factor of AFP level showed a significant correlation with GPC3-positive, which is consistent with previous studies.[33,34] Moreover, it was found that the levels of GPC3 mRNA in HCC tissue were correlated with the serum AFP level.[34] GPC3 and AFP may share the transcription factors zinc fingers, AFP regulator 2 (Arf2), and homeoboxes 2 (Zfh2), because some other tumors such as Yolksac tumors produce both AFP and GPC3.[35,36]

The radiomics signature comprised of all the selected radiomic features showed superior performance in predicting GPC3. In addition, the combined model integrated with clinical risk factors and a radiomics signature yielded improved performance remarkably. This suggested the complementary power of the radiomics and clinical signatures, which could be due to the fact that radiology can capture the phenotype of tumor at a macroscopic level, while the histopathology can provide the detailed quantification of underlying biological process at a microscopic level.
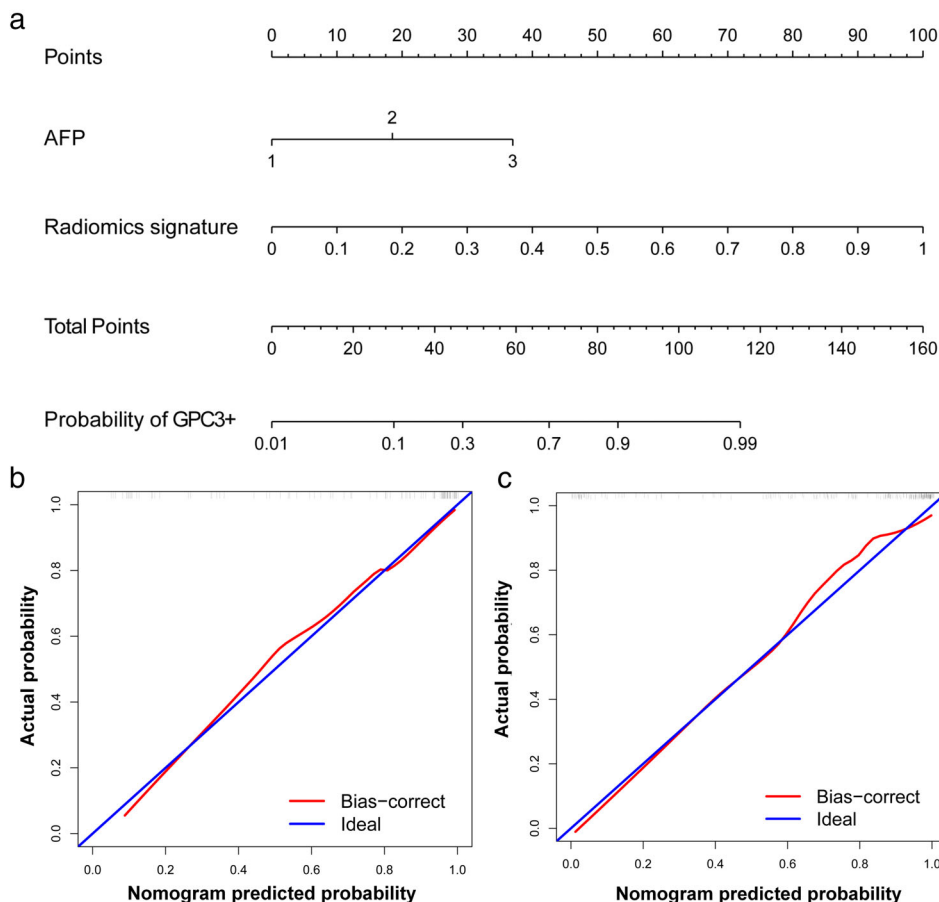
Finally, to explore clinical use, we provided the combined nomogram as an easy-to-use visual tool to calculate the predictive probability of GPC3-positive. According to the nomogram-predicted probability, patients could be stratified into high- and low-risk groups. For those patients with low risk, they can not only avoid unnecessary medical examination or therapy, but also reduce the burden of follow-up costs. Therefore, the nomogram could provide effective treatment guidance to assist clinicians for cancer management.

FIGURE 4: Nomogram and calibration analysis. (a) The nomogram based on the combined model incorporating clinical risk factor AFP and the radiomic signature. Calibration curves for the (b) training and (c) validation cohorts. The y-axis represents the actual rate of GPC3-postive in the patients; x-axis represents the nomogram-predicted probability of GPC3-positive. The blue diagonal solid line means an ideal agreement fitted by a perfect model
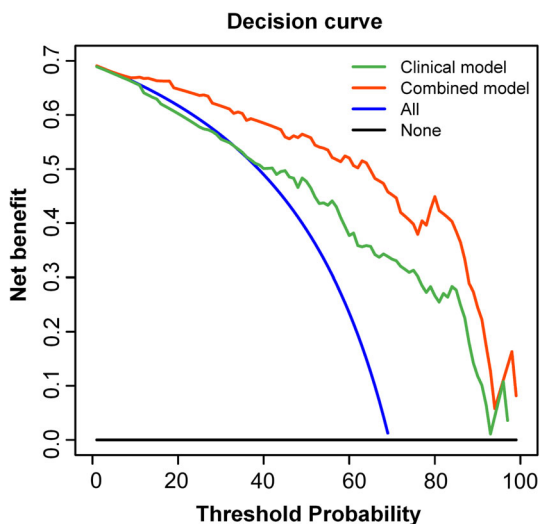
FIGURE 5: Decision curves for the combined model and clinical model in the training cohorts. The y-axis represents the net benefit; x-axis represents the threshold probability. The orange line measures the benefit for the combined model, and the green line measures the benefit for the clinical model. The blue and black lines represent the "treat all" and "treat none" strategies, respectively

Limitations

Our study has several limitations. First, as this is a single-center study, external validation through a multisite study is required to assess the generalizability of results. Secondly, we did not include genomic factors related with GPC3, which may provide additional information for GPC3 prediction. Lastly, it should be noted that the multimodal radiological data were not included in this research. In the future, MRI and CT data could be incorporated to explore the predicted performance of GPC3.

Conclusion

Our study shows that a radiomics signature based on contrast-enhanced MR images can be used as a preoperative predictor for identifying GPC3-positive HCCs, which may enable clinicians to choose optimal and individual treatment strategies to improve clinical outcomes.

REFERENCES

1. Ferlay J, Soerjomataram I, Dikshit R, et al. Cancer incidence and mortality worldwide: sources, methods and major patterns in GLOBOCAN 2012. Int J Cancer 2015;136(5):359-386.

2. Imamura H, Matsuyama Y, Tanaka E, et al. Risk factors contributing to early and late phase intrahepatic recurrence of hepatocellular carcinoma after hepatectomy. J Hepatol 2003;38(2):200-207.

3. Filmus J. Glypicans in growth control and cancer. Glycobiology 2001;11(3):19-23.

4. Filmus J, Selleck SB. Glypicans: Proteoglycans with a surprise. J Clin Invest 2001;108(4):497-501.

5. Capurro M, Wanless IR, Sherman M, et al. Glypican-3: A novel serum and histochemical marker for hepatocellular carcinoma. Gastroenterology 2003;125(1):89-97.

6. Ning S, Bin C, Na H, et al. Glypican-3, a novel prognostic marker of hepatocellular cancer, is related with postoperative metastasis and recurrence in hepatocellular cancer patients. Mol Biol Rep 2012;39(1):351-357.

7. Lai JP, Sandhu DS, Yu C, et al. Sulfatase 2 up-regulates glypican 3, promotes fibroblast growth factor signaling, and decreases survival in hepatocellular carcinoma. Hepatology 2008;47(4):1211-1222.

8. Magistri P, Leonard SY, Tang CM, Chan JC, Lee TE, Sicklick JK. The glypican 3 hepatocellular carcinoma marker regulates human hepatic stellate cells via hedgehog signaling. J Surg Res 2014;187(2):377-385.

9. Haruyama Y, Kataoka H. Glypican-3 is a prognostic factor and an immunotherapeutic target in hepatocellular carcinoma. World J Gastroenterol 2016;22(1):275-283.

10. Jana M, Gamanagatti S. Transjugular liver biopsy: Tips and tricks. Trop Gastroenterol 2012;33(3):168-172.

11. Sorrentino P, D'Angelo S, Tarantino L, Ferbo U, Bracigliano A, Vecchione R. Contrast-enhanced sonography versus biopsy for the differential diagnosis of thrombosis in hepatocellular carcinoma patients. World J Gastroenterol 2009;15(18):2245-2251.

12. Chen M, Li G, Yan J, et al. Reevaluation of glypican-3 as a serological marker for hepatocellular carcinoma. Clin Chim Acta 2013;423:105-111.

13. Nakatsura T, Yoshitake Y, Senju S, et al. Glypican-3, overexpressed specifically in human hepatocellular carcinoma, is a novel tumor marker. Biochem Biophys Res Commun 2003;306(1):16-25.

14. Liu H, Li P, Zhai Y, et al. Diagnostic value of glypican-3 in serum and liver for primary hepatocellular carcinoma. World J Gastroenterol 2010;16(35):4410-4415.

15. Aerts H, Velazquez ER, Leijenaar RTH, et al. Decoding tumour phenotype by noninvasive imaging using a quantitative radiomics approach. Nat Commun 2014;5(1):1-9.

16. Lambin P, Leijenaar RTH, Deist TM, et al. Radiomics: The bridge between medical imaging and personalized medicine. Nat Rev Clin Oncol 2017;14(12):749-762.

17. Scalco E, Rizzo G. Texture analysis of medical images for radiotherapy applications. Br J Radiol 2017;90(1070):20160642.

18. Castellano G, Bonilha L, Li LM, Cendes F. Texture analysis of medical images. Clin Radiol 2004;59(12):1061-1069.

19. McLaren CE, Chen WP, Nie K, Su MY. Prediction of malignant breast lesions from MRI features: A comparison of artificial neural network and logistic regression techniques. Acad Radiol 2009;16(7):842-851.

20. Yu JY, Zhang HP, Tang ZY, et al. Value of texture analysis based on enhanced MRI for predicting an early therapeutic response to transcatheter arterial chemoembolisation combined with high-intensity focused ultrasound treatment in hepatocellular carcinoma. Clin Radiol 2018;73(8):758.e9-758.e18.

21. Chen MD, Zhang J, Yang GX, Lin JM, Feng YQ. Differential diagnosis of hepatocellular carcinoma and hepatic hemangiomas based on radiomic features of gadoxetate disodium-enhanced magnetic resonance imaging. Nan Fang Yi Ke Da Xue Xue Bao 2018;38(4):428-433.

22. Zhou W, Zhang L, Wang K, et al. Malignancy characterization of hepatocellular carcinomas based on texture analysis of contrast-enhanced MR images. J Magn Reson Imaging 2017;45(5):1476-1484.

23. Yang L, Gu D, Wei J, et al. A Radiomics Nomogram for Preoperative Prediction of Microvascular Invasion in Hepatocellular Carcinoma. Liver cancer 2019;8(5):373-386.

24. Zwanenburg A, Leger S, Vallières M, Löck S. Image biomarker standardisation initiative. arXiv preprint arXiv:1612.07003, 2016.

25. Kramer AA, Zimmerman JE. Assessing the calibration of mortality benchmarks in critical care: The Hosmer-Lemeshow test revisited. Crit Care Med 2007;35(9):2052-2056.

26. Vickers AJ, Elkin EB. Decision curve analysis: A novel method for evaluating prediction models. Med Decis Making 2006;26(6):565-574.

27. Schisterman EF, Perkins NJ, Liu A, Bondell H. Optimal cut-point and its corresponding Youden index to discriminate individuals using pooled blood samples. Epidemiology 2005;16:73-81.

28. Filmus J, Church JG, Buick RN. Isolation of a cDNA corresponding to a developmentally regulated transcript in rat intestine. Mol Cell Biol 1988;8(10):4243-4249.

29. Fu SJ, Qi CY, Xiao WK, Li SQ, Peng BG, Liang LJ. Glypican-3 is a potential prognostic biomarker for hepatocellular carcinoma after curative resection. Surgery 2013;154(3):536-544.

30. Yasuda E, Kumada T, Toyoda H, et al. Evaluation for clinical utility of GPC3, measured by a commercially available ELISA kit with Glypican-3 (GPC3) antibody, as a serological and histological marker for hepatocellular carcinoma. Hepatol Res 2010;40(5):477-485.

31. Gillies RJ, Kinahan PE, Hricak H. Radiomics: Images are more than pictures, they are data. Radiology 2016;278(2):563-577.

32. Ng F, Kozarski R, Ganeshan B, Goh V. Assessment of tumor heterogeneity by CT texture analysis: Can the largest cross-sectional area be used as an alternative to whole tumor analysis? Eur J Radiol 2013;82(2):342-348.

33. Saito S, Ojima H, Ichikawa H, Hirohashi S, Kondo T. Molecular background of alpha-fetoprotein in liver cancer cells as revealed by global RNA expression analysis. Cancer Sci 2008;99(12):2402-2409.

34. Hsu HC, Cheng W, Lai PL. Cloning and expression of a developmentally regulated transcript MXR7 in hepatocellular carcinoma: Biological significance and temporospatial distribution. Cancer Res 1997;57(22):5179-5184.

35. Morford LA, Davis C, Jin L, Dobierzewska A, Peterson ML, Spear BT. The oncofetal gene glypican 3 is regulated in the postnatal liver by zinc fingers and homeoboxes 2 and in the regenerating liver by alpha-fetoprotein regulator 2. Hepatology 2007;46(5):1541-1547.

36. Zynger DL, Everton MJ, Dimov ND, Chou PM, Yang XJ. Expression of glypican 3 in ovarian and extragonadal germ cell tumors. Am J Clin Pathol 2008;130(2):224-230.